

Annihilation γ Ray Background Characterization and Rejection for a Small Beta Camera Used for Tumor Localization During Surgery

Craig S. Levin, *Member, IEEE*, Martin P. Tornai, *Student Member, IEEE*,
Lawrence R. MacDonald, *Student Member, IEEE*, and Edward J. Hoffman, *Senior Member, IEEE*

Division of Nuclear Medicine and Biophysics, UCLA School of Medicine
Los Angeles, CA 90095-6948

Abstract

We have developed a miniature (1.2 cm^2) beta-ray camera prototype to assist a surgeon in locating the margins of a resected tumor. With this technique, one directly detects betas emitted from exposed radio-labeled tissue. When imaging positron emitting radiopharmaceuticals, annihilation gamma ray interactions in the detector can mimic those of the betas. The extent of the background contamination depends on the detector, geometry and the tumor specificity of the radiopharmaceutical. We have characterized the effects that annihilation gamma rays have on positron imaging with our small camera. We studied beta and gamma ray detection rates and imaging using small positron or electron sources directly exposed to the detector to simulate hot tumor remnants, and a cylinder filled with ^{18}F to simulate annihilation background from the brain. For various ratios of phantom head/tumor activity, a background gamma rate of $2.0 \text{ cts/sec}/\mu\text{Ci}$ was measured in the $\text{CaF}_2(\text{Eu})$ detector. We present two gamma-ray background rejection schemes that require a β - γ coincidence. The first configuration uses a high efficiency scintillator coincidence "shield", the second, a "phoswich". Results show that these coincidence methods work with $\sim 99\%$ gamma ray rejection efficiency.

I. INTRODUCTION

We have developed [1-11] miniature ($\leq 1.2 \text{ cm}^2$), gamma (γ) and beta (β) ray imaging scintillation camera prototypes for the purpose of assisting a surgeon in locating and removing the margins of a resected tumor. The β imaging device directly detects positrons (β^+) or electrons (β^-) emitted from radiolabeled tissue exposed during surgery. The short range of the β 's in tissue and detector and close proximity imaging of the activity (lesion) ensure high sensitivity and resolution with no need for a collimator. Imaging capabilities *in situ* help to distinguish signal from background and allow a relatively large area to be assayed in a relatively short time. Most of the pure β emitting radiopharmaceuticals readily available and used in the nuclear medicine clinic for tumor imaging are β^+ emitters (usually ^{18}F -labeled) for Positron Emission Tomography (PET). Using β^+ emitters, the detector will measure activity from annihilation γ rays (background) as well as from β^+ s (signal). The ability to extract the true β activity image from the total β and background γ signal depends on the ratio of tumor to background activity rates observed. This, in turn, depends on the radiopharmaceutical tumor uptake specificity. For tumor localization during Neurosurgery, a candidate radiopharmaceutical for use in conjunction with this surgical probe is ^{18}F -Fluorodeoxyuridine (FdUr). UCLA PET studies with this tracer have shown brain tumor to normal tissue uptake ratios as high as 10:1.

The detected β/γ rate ratio also depends on the γ ray efficiency of the scintillator. To minimize this background contamination, the scintillator chosen for the device is β sensitive, yet relatively γ ray insensitive (low Z, low density). The scintillator should be as thin as possible (for lower γ ray efficiency), but thick enough to stop most of the β rays from the source (for higher light output and sensitivity) [4, 5].

There are a few techniques one might use for gamma ray background (GRB) rejection for non-imaging β probes detecting β^+ s. One idea is to only accept those detected events above an energy threshold which corresponds to the Compton edge of the background γ ray spectrum [12]. This approach, however, has the problem of a greatly reduced sensitivity, since low energy β events (a large proportion of all events) will be cut out as well. In addition, due to relatively poor energy resolution, the Compton edge is ill-defined and may significantly spread into higher energies.

A second technique [13] employed with a non-imaging β detecting probe, uses a second concentric detector to estimate γ -only activity. Data is acquired simultaneously in both detectors and the β -only component is determined by subtracting the suitably weighted counts measured in the second detector from that counted in the first. The main disadvantages of this technique were that (1) a correct and precise determination of the weighting factor that is valid for all background γ ray source distributions is difficult and (2) the second detector was inefficient for γ rays.

In this work we propose two new "on-line" background rejection schemes for an imaging device, both of which use beta-gamma (β - γ) coincidence detection. GRB rejection is achieved by requiring a detected coincidence between $\text{CaF}_2(\text{Eu})$, the primary β detector, and an adjacent secondary detector that detects the associated γ ray. We will demonstrate the method using ^{18}F , a β^+ emitter used as a label for tumor detection in PET. With β^+ s there are two γ rays associated with each β event detected. The β - γ coincidence GRB rejection scheme is especially useful for β^+ annihilation GRB removal. Since two γ rays are emitted roughly 180° apart this ensures a high geometric efficiency for detection of at least one. However, this GRB rejection technique could, in principle, be useful for any β -emitting pharmaceutical (such as ^{131}I) that has an accompanying γ ray.

II. METHODS

A. Annihilation Background Characterization

Figure 1 shows the schematic of the basic experimental set-up used to characterize the effect of GRB on β detection and imaging with the surgical imaging probe. Details of the imaging device are described elsewhere [5]. Fiber optics read out the scintillation light from a 1.25 cm diameter $\text{CaF}_2(\text{Eu})$

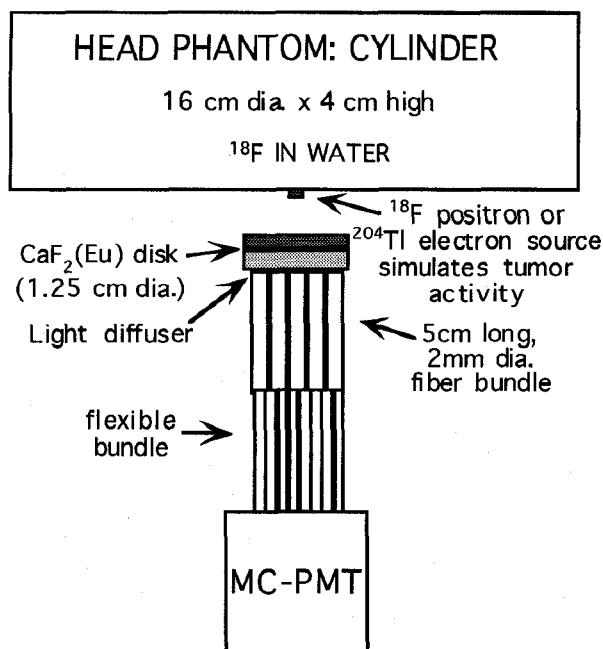


Figure 1. Schematic of set up to characterize GRB for the fiber optic-coupled miniature β -Ray Camera. A hot cylinder (^{18}F) with attached point source (^{18}F or ^{204}Tl) simulates head and tumor activities, respectively.

disk and guide it to a multi-channel photo-multiplier tube (MCPMT). The fiber optic readout cabling provides flexibility for the surgeon and isolates exposed tissue from the bulky MCPMT, electronics, and high voltage distributions. The MCPMT tube is read out with 4 electronic channels (x_+ , x_- , y_+ , y_-) using resistive charge division, and the detected events are positioned with the standard logic. The intrinsic resolution of the device is 0.5 mm FWHM. For background considerations, we want the detector to be as thin as possible, yet thick enough to stop a majority of the β 's (for higher light output and sensitivity). A $\text{CaF}_2(\text{Eu})$ thickness of ~ 0.5 - 0.7 mm is optimal ($Z_{\text{eff}} = 16.9$, $\rho = 3.17 \text{ g/cm}^3$) for low γ - and high β -ray detection efficiencies [4].

A near by cylindrical Lucite phantom (16 cm dia., 4 cm high, Fig. 1) filled with ^{18}F simulated the head γ ray activity distribution. Small ^{204}Tl (β^- , $E_{\text{max}}=765 \text{ keV}$, $\tau_{1/2}=3.8 \text{ yr}$) or ^{18}F (β^+ , $E_{\text{max}}=635 \text{ keV}$, $\tau_{1/2}=110 \text{ min}$) sources, fixed to the bottom of the cylinder, simulated the tumor site/surgical cavity activity.

For all measurements, the β and γ ray components of the total activity are determined by using the "beta shield" method. The contribution solely due to γ rays was measured by placing a thin, plastic β shield between the β source and the scintillator. The β activity is obtained by subtracting the decay corrected γ component from the total $\gamma+\beta$ signal, with the two data sets acquired for the same duration. The black plastic β shield was 5 mm thick.

Two experiments were performed to ascertain the effects of GRB on β ray detection and imaging. In the first measurement, the ^{204}Tl source (fixed activity for the duration of the experiment) was used to simulate the residual tumor activity. The source was collimated in a 2 mm spot on the center of a 0.8 mm thick $\text{CaF}_2(\text{Eu})$ disk with a collimated activity of approximately 60 nCi. An initial activity of approximately 1 mCi of ^{18}F was placed in the cylindrical head

phantom with volume of roughly 800 cm^3 . The total activity was measured as a function of time. This experiment is useful since it demonstrates the effects of GRB for various ratios of detected γ/β rates.

The second experiment utilized the U-C-L-A #1 copper β transmission phantom [5] (see top of Fig. 6) to characterize the effects of GRB on imaging. The phantom lettering is composed of 61, 0.5 mm holes drilled in 0.4 mm thick copper, spaced 0.6 mm apart. The copper mask was placed directly on top of the detector. The cylindrical phantom, filled with ^{18}F was placed 3 cm from the top of the imaging probe and copper mask. For β^+ 's, a cotton swab saturated with ^{18}F was used to simulate the exposed tumor. The ^{18}F cylinder γ activity and source β^+ activity passing through the UCLA phantom were imaged.

B. β - γ Coincidence Background Rejection

Figure 2 depicts two "on-line" annihilation GRB rejection techniques, both of which utilize the $\beta^+-\gamma$ coincidence technique. Requiring a β^+ hit in the $\text{CaF}_2(\text{Eu})$ in coincidence with an annihilation γ ray hit in a nearby detector that is shielded from direct β interactions, and efficient for γ rays, will allow us to separate true β^+ events from background. The "gamma annulus" approach (Fig. 2a) utilizes a secondary γ ray efficient scintillator that completely surrounds the front end of the imaging probe. With the "annulus" geometry, at least one of the two back-to-back annihilation γ rays resulting from a β^+ stopping in the $\text{CaF}_2(\text{Eu})$ has a high probability of interacting with the annulus, no matter where the β^+ annihilation occurs within the $\text{CaF}_2(\text{Eu})$. In principal, for a very long annulus surrounding the detector, this would imply 4π coverage (only 2π coverage is required to detect at least one from the pair). The event will be recorded as a true β^+ event only if there is a coincidence between the two detectors. Another process that could mimic this dual hit signature would be a Compton scatter in the $\text{CaF}_2(\text{Eu})$ followed by a photoabsorption in the γ ray detector. This secondary process is unlikely since there are two γ -ray interactions required (one in a low density, low Z material), compared to only one for the desired $\beta^+-\gamma$ event (an incoming β^+ will always interact in the $\text{CaF}_2(\text{Eu})$). The U-C-L-A letter transmission phantom was used to determine the efficiency of this background rejection scheme.

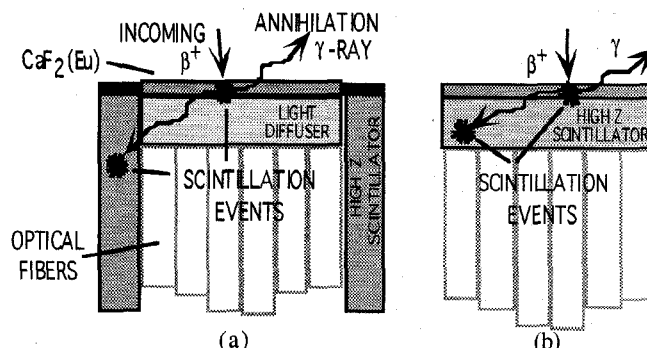


Figure 2. Schematic of two on-line $\beta^+-\gamma$ coincidence annihilation background rejection techniques. (a) The "gamma annulus" approach utilizes a secondary high Z , high density scintillator surrounding the imaging probe front end. (b) The "phoswich" approach, uses the γ ray detector "sandwiched" between the $\text{CaF}_2(\text{Eu})$ and the fibers. Only front portion is shown (see Fig. 1). A thin shield surrounds the sides of both configurations to prevent a direct β^+ interaction in the γ detector.

The "phoswich" [14, 15] approach (Fig. 2b), uses a γ ray efficient detector (assume GSO, for example) that is both much faster than $\text{CaF}_2(\text{Eu})$, and is transparent to its blue scintillation light. This scintillator is "sandwiched" between the $\text{CaF}_2(\text{Eu})$ and the fiber bundle. The GSO serves the dual purpose of the fast γ -ray detector and the light diffuser required for the continuous $\text{CaF}_2(\text{Eu})$ scintillator imaging [4,5].

In the phoswich configuration, the differences in both decay time and light output between the $\text{CaF}_2(\text{Eu})$ (slow decay $\sim 1 \mu\text{s}$) and the GSO (fast decay, 60 ns) allows one to use pulse shape discrimination methods to identify the coincident events of interest. The events are clearly distinguishable because the decay times of the two scintillators differ by more than a factor of 10. An annihilation γ ray associated with the β^+ of interest will very likely traverse the secondary detector and a good event will have a signature of two added pulses: one slow ($\text{CaF}_2(\text{Eu})$) and one fast (GSO). By triggering on the rise of the fast decay portion of the signal, delaying by the decay time of that pulse (typically $< 200 \text{ ns}$), and then integrating the slow portion of the pulse, nearly 90% of the true β^+ signal will be extracted. This is accomplished with the use of a fast leading edge or constant fraction discriminator, set above the $\text{CaF}_2(\text{Eu})$ amplitudes, to trigger a linear gate for the amplified positioning signals of the imaging probe. The linear gate is normally closed and will open with a delayed signal from the γ ray detector trigger. This technique works best with high efficiency detectors that are both fast and have high light yield.

As with essentially all background rejection schemes, the $\beta^+ \text{-}\gamma$ coincidence method results in an overall reduction in sensitivity. The extent of reduction depends on the detection efficiency of the γ ray detector. In principal, if that detector has a high stopping power for 511 keV γ rays, and subtends a large solid angle to the $\text{CaF}_2(\text{Eu})$ (see Fig. 2), for all positions within the $\text{CaF}_2(\text{Eu})$, the coincident sensitivity of the system will be acceptable.

For both $\beta^+ \text{-}\gamma$ coincidence rejection schemes, the efficiency of the γ ray rejection can be measured by comparing the detected γ/β ratio with and without the $\beta^+ \text{-}\gamma$ coincidence. (recall the γ/β ratio is measured using a "beta-shield"). In addition, if we block the β 's from the $\text{CaF}_2(\text{Eu})$ during coincidence acquisition, the resulting events seen are due to the background $\gamma \text{-}\gamma$ process (for example, a Compton scatter in the $\text{CaF}_2(\text{Eu})$ followed by a photoabsorption in the adjacent γ ray detector). The number of coincident events measured with the β absorber in place compared to that without, when the two data sets are acquired for an equal amount of time (with decay correction), determines how often two γ ray interactions mimic a $\beta^+ \text{-}\gamma$ event.

III. RESULTS

A. Beta and Annihilation Gamma Ray Activity Rates

Figure 3 shows $\gamma + \beta$, γ and β spectra measured for different ^{18}F cylinder activity levels (simulating head activity) with an attached ^{204}Tl β source (simulating residual tumor activity). We see that even for this very thin $\text{CaF}_2(\text{Eu})$ disk (0.8 mm thick, 1.25 diameter) that the GRB detection rate is significant. For the second through fourth spectra, the γ component dominates the measured activity. As the activity in the phantom decays, the constant ^{204}Tl activity (beta spec-

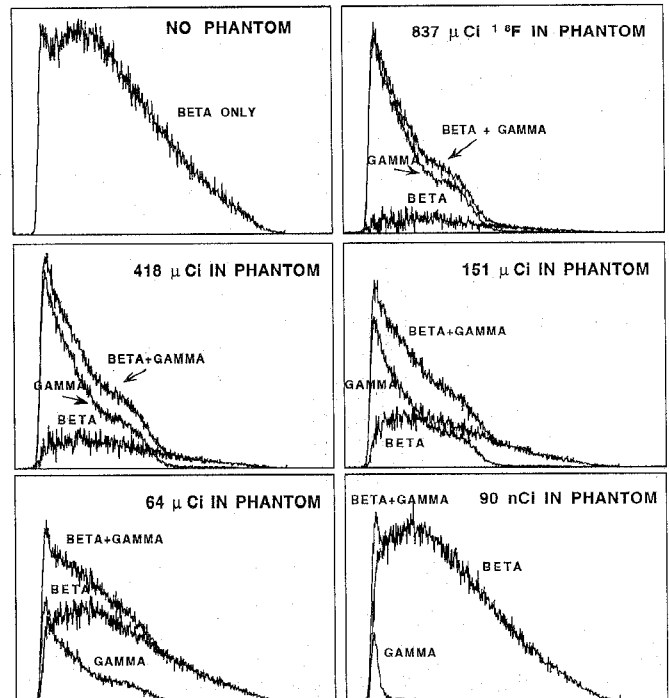


Figure 3. Some $\gamma + \beta$, γ and β activities measured for various ^{18}F phantom activity levels (^{204}Tl β source). The need for annihilation GRB rejection is evident. See Figure 4.

trum) emerges. The need for annihilation GRB rejection is evident.

Figure 4 displays the measured annihilation γ ray (from ^{18}F phantom) to β (collimated ^{204}Tl) rate ratio in the $\text{CaF}_2(\text{Eu})$ as a function of phantom head to tumor activity (not concentration) ratio. As expected, the β rate was constant and the γ rate varies linearly with phantom activity. A γ rate of 1.8 cts/sec/ μCi from the phantom was measured. For this measurement, the activity from the collimated ^{204}Tl β source corresponded to approximately 60 nCi which yielded a constant detected β activity rate of roughly 4500 cts/sec/ μCi . However, for accurate β^+ imaging during surgery, what is important is the ratio of the γ and β rates, not the absolute rates. Depending on the tumor affinity of the tracer used, the actual γ/β ratio expected for a tumor will lie somewhere on the curve of Figure 4. For example, assume the 800 g cylinder properly estimates the mass of the brain and the 60 nCi β source roughly simulates a 10 mg piece of residual tumor. A 10:1

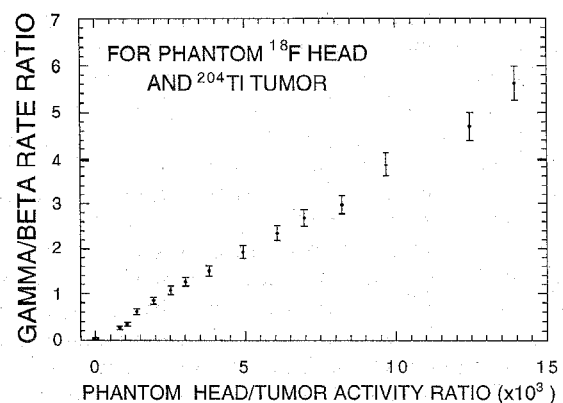


Figure 4. Measured annihilation γ (^{18}F) to β (^{204}Tl) rate ratio in the camera front end as a function of phantom head to tumor activity ratio (see Fig. 1). The collimated ^{204}Tl β source corresponded to approximately 60 nCi.

tumor (β source) to head (cylinder) uptake by volume (e.g. using FdUr) implies $\sim 480 \mu\text{Ci}$ in the head (cylinder). From Figure 4, this implies an expected activity γ/β rate ratio of approximately 3:1, which means some sort of GRB rejection scheme may be necessary. To reiterate, the relative, rather than absolute, residual tumor to head activity levels is the important quantity. For lower tumor to tissue uptake ratios the GRB problem will be worse (γ/β rate ratio will be higher).

For $\text{CaF}_2(\text{Eu})$ thickness $< 1.6 \text{ mm}$, ^{18}F flood irradiation studies showed both the γ and γ/β activity to increase linearly with thickness. Figure 5 shows the results for the ratio of detected γ to β rates as a function of several ratios of ^{18}F phantom head to ^{18}F tumor activity levels for a 0.8 mm thick detector. The extent of GRB contamination for a given ^{18}F tumor seeking radiopharmaceutical can be determined from this figure, once the brain to tumor activity is known. For example, a phantom head/tumor activity ratio of 4000:1 implies that the detected γ/β ratio is approximately 1.3:1. The detected γ rate was roughly 2.0 cts/sec/ μCi for this measurement which compares well to the ^{204}Tl measurement of Figure 4. Note that for the γ/β detected rates as a function of head/tumor concentration instead of activity ratio, one must know the approximate tumor volume.

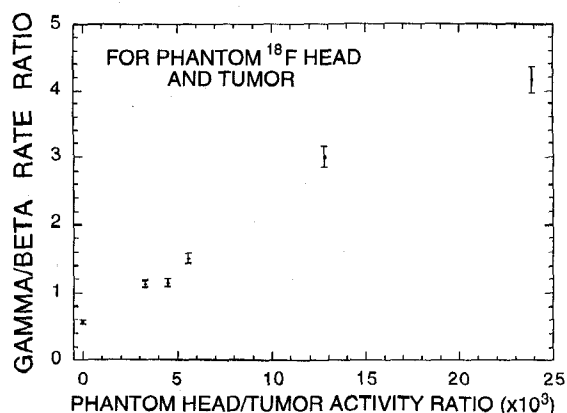


Figure 5. γ/β detected rate ratio as a function of various ^{18}F cylinder /source (simulating head/tumor) activity levels.

B. Effect of Annihilation γ Rays on Beta Imaging

Figure 6 demonstrates the potential problem of annihilation GRB for β imaging with this camera. Images were obtained using the U-C-L-A #1 copper transmission phantom (shown at top) on the β imaging probe irradiated with $100 \mu\text{Ci}$ of either ^{204}Tl (β^- s, left image) or ^{18}F (β^+ s, right image). The ^{18}F image shown was acquired with no activity in the head phantom so it represents the best case scenario in terms of GRB. The potential need for annihilation background rejection is evident. The presence of β^+ annihilation GRB generated within the cotton swab, and/or the $\text{CaF}_2(\text{Eu})$ is evident as a loss of contrast in the right compared to the left (pure β) image. The energy spectra of the particle components forming the images are shown below each image. Again, the extent of GRB contamination depends on the tumor-seeking radio-pharmaceutical specificity.

Figure 7 shows ^{18}F transmission images for a few phantom head to tumor activity ratios. We estimated "tumor activity" in the context of transmission phantom imaging by calculating the fraction of the exposed β activity from the ^{18}F

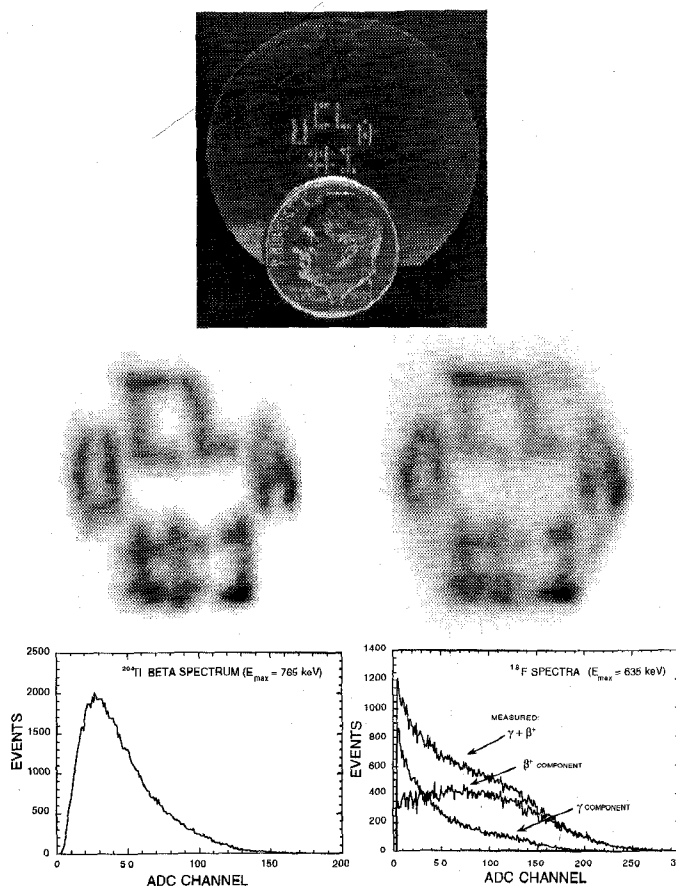


Figure 6. U-C-L-A copper transmission phantom (top) on the β imaging probe irradiated with $100 \mu\text{Ci}$ of either ^{204}Tl (β^- s, left image) or ^{18}F (positrons, right image). The presence of annihilation γ ray background is evident as a loss of contrast in the right compared to the left (pure β) image. The corresponding β^- or β^+ , γ and combined spectra are shown beneath.

cotton swab that passes through the transmission phantom. For an activity ratio of 3000:1 the corresponding γ/β activity ratio detected is roughly 1:1 (from Fig. 5) and the phantom lettering is clearly visible above the background. For an activity ratio of 12000:1, the corresponding γ/β rate is 3:1 and the lettering is unresolved.

Figure 8 demonstrates the β -shield technique for γ -ray background rejection. The activity passing through the copper UCLA β^+ transmission phantom was consistent with a 3% tumor/tissue activity ratio. This activity ratio was chosen from an analysis of previous UCLA PET studies of tumor FdUr uptake in the brain. This ratio underestimates the true γ/β activity ratio we would measure with our device since tumor self-absorption of betas was not taken into account. The top left image shows the resulting image with this realistic β^+ to γ ray source ratio with no shield present (β^+ s + γ rays). The top right image shows the β^+ shielded result (on-

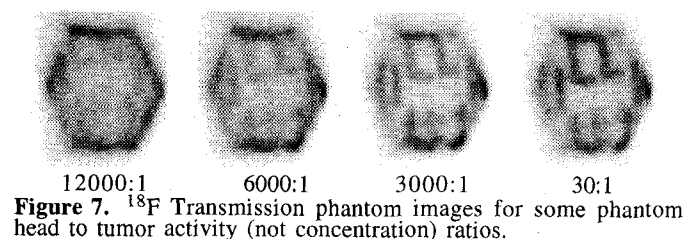


Figure 7. ^{18}F Transmission phantom images for some phantom head to tumor activity (not concentration) ratios.

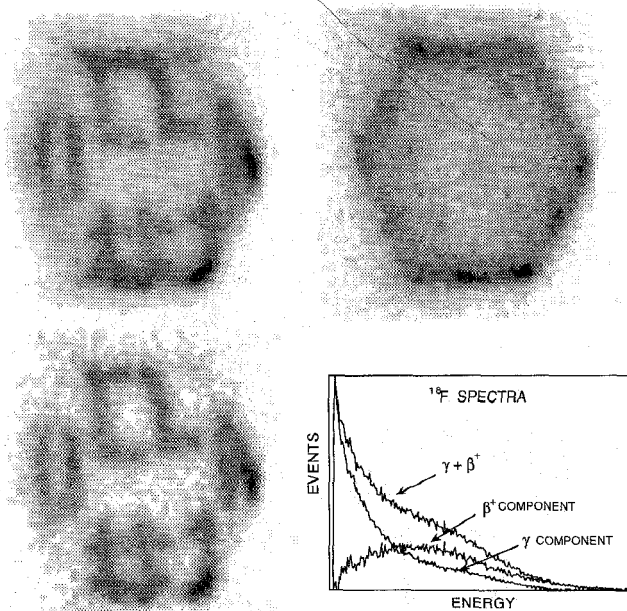


Figure 8. The " β -shield" technique for γ -ray background rejection. Top left: β^+ s + γ rays (unshielded). Top right: γ rays only (shielded). Bottom left: β^+ s only (obtained by subtracting the γ -ray only component from the unshielded image). Note the improvement in contrast. Right: corresponding energy spectra.

ly γ -rays). The bottom left image shows that obtained by subtracting the γ -ray only component from the unshielded image (resulting in β only). Note the improvement in contrast after subtraction (and reduction in counts). The various energy spectra ($\gamma+\beta$, γ and β) are shown in the bottom right graph. Unfortunately, it may not be possible for a surgeon using this imaging device to either insert a β shield or hold the device long enough to make two images. An on-line background rejection scheme would be preferable.

C. β - γ Coincidence Background Rejection

In Figure 9 we show images obtained with both the β -shield and the "on-line" β - γ coincidence background rejection

method. A prototype of the "gamma annulus" β - γ coincidence method depicted in Fig. 2b was used to acquire the right-most image. This prototype consisted of a partial BGO coincidence shield (not full annulus), subtending 0.2π at the $\text{CaF}_2(\text{Eu})$ detector. This partial shield was constructed using 3, 30 mm x 20 mm x 5 mm thick rectangular pieces of BGO, covered in 5 layers of white teflon tape. 2 mm plastic strips were used to shield the BGO from direct β^+ irradiation. The partial BGO coincidence "shield" was read out with a separate PMT. This shield was configured around the camera front end, similar to that shown in Fig. 2b. Although non-ideal, this BGO shield was used to demonstrate the high GRB rejection efficiency obtained by requiring a β - γ coincidence. For this measurement the activity used in the phantom head and that passing through the UCLA transmission phantom from the cotton swab tumor were again roughly consistent with the 3% tumor/tissue activity ratio. The β camera and the BGO shield were set in coincidence for image acquisition.

The energy spectrum corresponding to the measured $\text{CaF}_2(\text{Eu})$ activity seen in each image of Figure 9 is shown underneath. We see from both the images and spectra that the β - γ coincidence method appears to be at least as efficient (and perhaps better) in restoring the contrast as the β -shield method. Restoring the image contrast is equivalent to removing the γ ray component and leaving the β^+ component; Compare the far right image of Figure 9 to the ^{204}Tl image in Figure 6 that has no GRB present. The measured relative β , γ , and $\gamma + \beta$ ray detection rates ratio from the first three images were 1:1.6:2.6, respectively. The γ ray rejection efficiency (defined at the end of Section II) of this β - γ coincidence technique was measured to be 98.5%. The γ - γ contribution was $< 2\%$ of the β - γ coincidences. The detected β - γ coincidence activity rate was a factor of 15 lower than the combined β and γ rate when not in coincidence. This lower count rate is consistent with (1) the fact that the partial BGO shield subtended only 0.2π at the center of the $\text{CaF}_2(\text{Eu})$ disk, and (2) if a γ ray traversed the BGO shield, the overall probability of interacting was estimated to be between 0.4 and 0.97 for the given geometry, depending on the entrance angle.

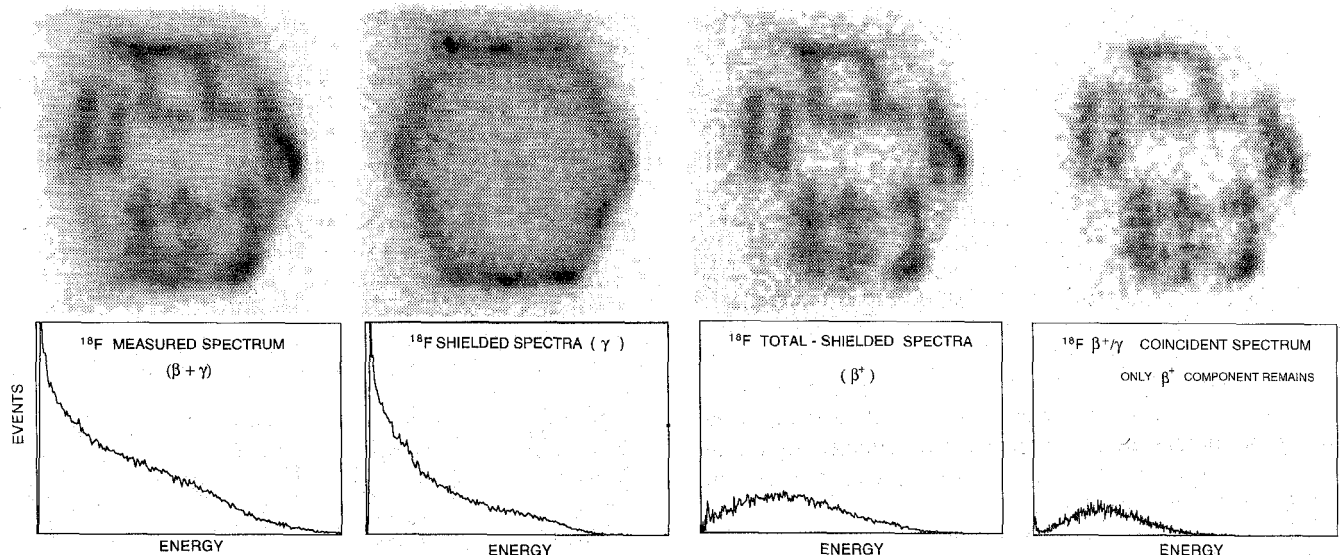


Figure 9. From left to right in the figure: (1) the β^+ + γ ray background; (2) the β shielded γ ray component only; (3) the difference between the two previous figures = the β^+ only component; (4) the same image acquired with the probe and BGO shield in coincidence. The energy spectra measured in the $\text{CaF}_2(\text{Eu})$ for each case are shown below the image.

In Figure 10 we show typical detected digital oscilloscope PMT signals from the $\text{CaF}_2(\text{Eu})$ -GSO phoswich detector configuration with ^{18}F as the source of both β^+ s and annihilation γ rays. The GSO (~ 60 ns decay time) pulse from the PMT has a sharp rise and fall and the $\text{CaF}_2(\text{Eu})$ (~ 1 μs decay time) signal has a long tail. In Fig. 10a, we see the slow $\text{CaF}_2(\text{Eu})$ decay from a β^+ hit. Fig. 10b shows only the fast GSO signal from an annihilation γ ray interaction. We chose the criterion that a hit in both the $\text{CaF}_2(\text{Eu})$ (slow decay component) and the GSO (fast decay component), with a maximum amplitude greater than 30 mV signified the desired $\beta^+-\gamma$ coincidence event. In Fig. 10c, we show such an event. By triggering on a high leading edge pulse, delaying for 200 ns and setting the linear gate on the slow component, the desired $\beta^+-\gamma$ coincidence events can be identified and used for imaging. The linear gate was set as indicated in Fig. 10c, with roughly 90% the spectrum in Figure 10a passing the gate. This portion of the pulse went into a shaping amplifier and was digitized. The time integrated light yield of $\text{CaF}_2(\text{Eu})$ is a factor of 2.5 greater than for GSO.

Another γ ray detector candidate is LSO which has 3 times the light yield, is 1/3 faster, and has a higher stopping power than GSO. In Fig. 10c the GSO signal is roughly 3 times the $\text{CaF}_2(\text{Eu})$ maximum. The LSO would potentially push this number to a factor of 10. The LSO has a natural component of radioactivity (~ 700 keV β , 200 and 310 keV γ) which would contribute on the order of 50 cps to the γ rate in LSO. With a coincidence requirement and since we expect low $\text{CaF}_2(\text{Eu})$ data rates (< 1000 cps), this would not be a problem.

Figure 11 shows measured energy spectra of ^{18}F in the $\text{CaF}_2(\text{Eu})$ -GSO phoswich detector. The delayed linear gate technique successfully discriminates between pure GSO events, pure $\text{CaF}_2(\text{Eu})$ events and superimposed events from both scintillators. In (a) both β shielded and unshielded ($\beta+\gamma$) spectra are shown without any pulse shape discrimination. Note that the pulse height of $\text{CaF}_2(\text{Eu})$ in Fig. 11a is approximately a factor of 2.5 greater than for GSO. In (b) only the slow component ($\text{CaF}_2(\text{Eu})$) of the phoswich signals is integrated (1.5 μs shaping time) and digitized using the delayed linear gate technique. This results in a large reduction of the fast GSO component (γ ray) and enhancement of the $\text{CaF}_2(\text{Eu})$ (β^+) portion. Here the gate width was set at 1.5 μs (200 ns delay). We required that the desired superimposed $\text{CaF}_2(\text{Eu})$ -GSO scintillation signals to have a fast and relatively high amplitude leading edge. As expected, the γ/β^+ events ratio in $\text{CaF}_2(\text{Eu})$ decreases with increasing leading edge discriminator threshold. For a 50 keV threshold, the dual event (coincidence) phoswich GRB rejection efficiency was measured to be 98.6%. Without coincidence, the detected γ/β rate ratio was 4.8:1. With the coincidence acquisition, the $\gamma-\gamma$ contribution was $\sim 6\%$ of the $\beta-\gamma$ events. We do not yet understand the peculiar shape of the β component spectrum in Figure 11b, but we attribute it to the presence of the GSO. In Figure 11c the delay was set to zero, the gate width set to 300 ns, and only the GSO (γ hit) component was integrated (250 ns shaping time) and digitized. Note the near absence of the $\text{CaF}_2(\text{Eu})$ component.

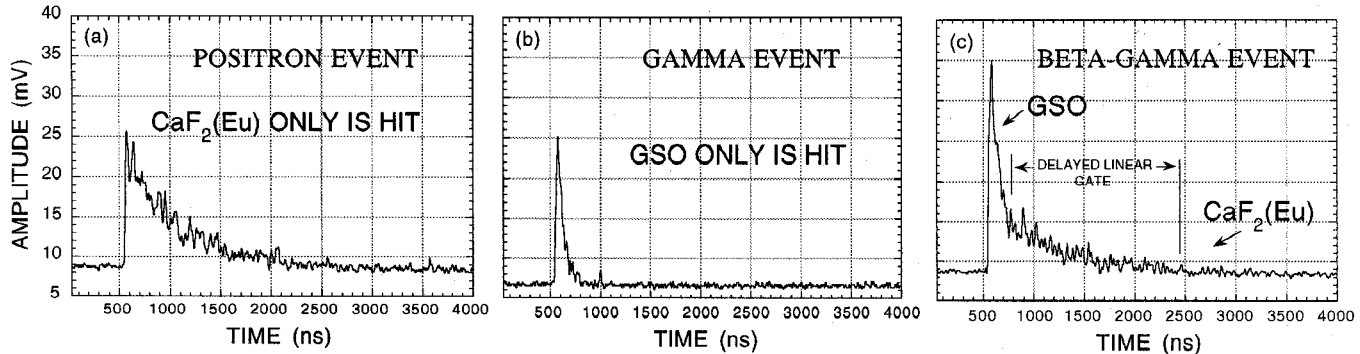


Figure 10. Typical detected β^+ annihilation digital oscilloscope PMT signal traces from the $\text{CaF}_2(\text{Eu})$ -GSO phoswich detector using ^{18}F as the source of β^+ s and annihilation gamma ray background. (a) a hit in only the $\text{CaF}_2(\text{Eu})$ component (~ 1 μs decay time), (b) a hit in only the GSO component (~ 60 ns decay time), indicative of a gamma-ray interaction, and (c), A hit in both the $\text{CaF}_2(\text{Eu})$ (slow decay component) and GSO (fast component), with amplitude greater than 30 mV signifies the desired $\beta^+-\gamma$ coincidence.

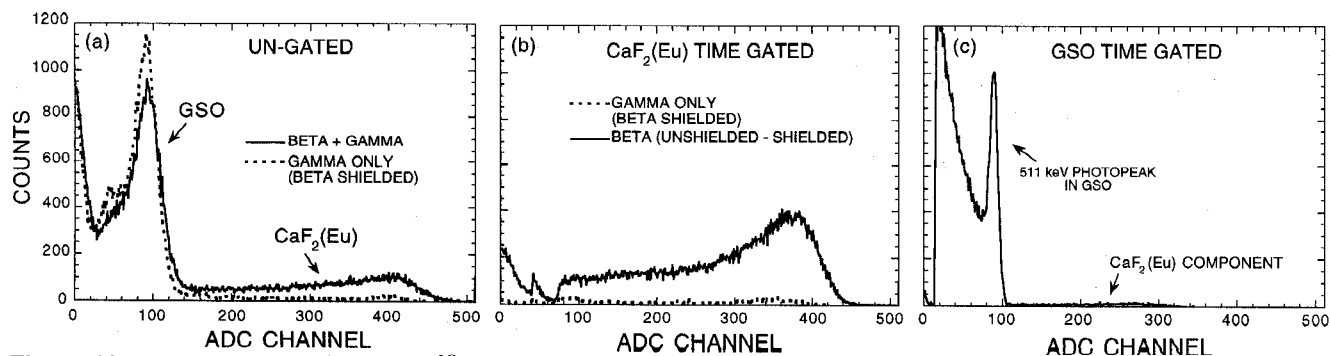


Figure 11. Measured energy spectra of ^{18}F in the $\text{CaF}_2(\text{Eu})$ -GSO phoswich detector. (a) both beta shielded and unshielded ($\beta+\gamma$) spectra are shown without any pulse shape discrimination; (b) only the slow component ($\text{CaF}_2(\text{Eu})$) of the phoswich signals is integrated and digitized using the "delayed linear gate" technique, resulting in large reduction of fast GSO component (gamma ray interactions) and enhancement of the $\text{CaF}_2(\text{Eu})$ (β^+) component; (c) the delay was set to zero and the gate width is set to 300 ns and only the gamma ray GSO component was integrated and digitized.

IV. SUMMARY AND CONCLUSION

We have characterized the annihilation gamma ray background problem for our surgical β ray camera. The extent of the problem depends on the specific tumor uptake of the chosen radiopharmaceutical. This tumor to normal tissue uptake ratio determines the relative detected rates of β and gamma rays. For a realistic source activity ratio in a simulated tumor and head phantom, we observed that the annihilation gamma ray background potentially can be a problem for imaging, even for the very thin scintillator used. Fairly complex images acquired with an β transmission phantom showed a significantly reduced contrast when imaging β^+ s vs. β^- s due to the background annihilation gamma rays randomly interacting within the detector. Two beta-gamma coincidence rejection methods were investigated. Both methods were $> 98\%$ efficient for gamma ray rejection and restored image contrast significantly. As with any background removal process, using coincidence acquisition reduced the count rate. This reduction is minimized with the use of a highly efficient (geometric and intrinsic) gamma ray absorber. Although the technique was demonstrated with β^+ s and annihilation GRB, in principle, it may be applied to imaging any radiopharmaceutical beta source that has an associated background γ ray present. However, because of the two collinear annihilation gamma rays, the coincidence sensitivity will be the highest for β^+ imaging.

V. ACKNOWLEDGMENTS

This work was supported in part by grants from the Department of Energy (DE-FCO3-87-ER 60615), National Institutes of Health (R01-CA56655), (R01-CA61037) and the State of California (IRB-0225). The authors acknowledge Dr. Mark Hanson of the UCLA Physics Department for the use of his digital oscilloscope.

VI. REFERENCES

- [1] B.E. Patt, J.S. Iwanczyk, M.P. Tornai, C.S. Levin, and E.J. Hoffman. Development of a Mercuric Iodide Detector Array for Medical Imaging Applications. *Nucl. Instr. & Meth. A* **366** (1995) 173-182.
- [2] L.R. MacDonald, M.P. Tornai, C.S. Levin, J. Park, M. Atac, D.B. Cline, E.J. Hoffman. Investigation of the Physical Aspects of Beta Imaging Probes Using Scintillating Fibers and Visible Light Photon Counters. *IEEE Trans. Nucl. Sci.* **42-4** (1995)1351-1357.
- [3] L.R. MacDonald, M.P. Tornai, C.S. Levin, J. Park, M. Atac, D.B. Cline, E.J. Hoffman. Small Area, Fiber Coupled Scintillation Camera for Imaging Beta-Ray Distributions Intra-Operatively. In *Photoelectronic Detectors, Cameras and Systems*, Eds. C.B. Johnson, E.J. Fenyves, *Proceedings of the SPIE* **2551** (1995) 92-101.
- [4] C.S. Levin, L.R. MacDonald, M.P. Tornai, E.J. Hoffman, J. Park. Optimizing Light Collection from Thin Scintillators Used in a Beta-Ray Camera for Surgical Use. *IEEE Trans. Nucl. Sci.* **43-3** (1996) 2053-60.
- [5] M.P. Tornai, L.R. MacDonald, C.S. Levin, S. Siegel, E.J. Hoffman. Design Considerations and Initial Performance of a 1.2 cm² Beta Imaging Intra-Operative Probe. *IEEE Trans. Nucl. Sci.* **43-4** (1996) 2326-2335.
- [6] M.P. Tornai, E.J. Hoffman, C.S. Levin, L.R. MacDonald. Characterization of Fluor Concentration and Geometry in Organic Scintillators for *In Situ* Beta Imaging. *IEEE Trans. Nucl. Sci.* **43-6** (1996) 3342-7.
- [7] M.P. Tornai, L.R. MacDonald, C.S. Levin, S. Siegel, E.J. Hoffman, J. Park, M. Atac, D.B. Cline. Miniature Nuclear Emission Imaging System for Intra-operative Applications. In *Proceedings from UCLA International Conference on Imaging Detectors in High Energy & Astroparticle Physics*, World Scientific Publishing, 1996.
- [8] E.J. Hoffman, M.P. Tornai, C.S. Levin, L.R. MacDonald, and S. Siegel. Gamma and beta intra-operative imaging probes. *Nucl. Instr. Meth. A* (in press).
- [9] E.J. Hoffman, M.P. Tornai, C.S. Levin, L.R. MacDonald, and S. Siegel. Design and Performance of Gamma and Beta Intra-Operative Imaging Probes. *Physica Medica* (in press).
- [10] M.P. Tornai, C.S. Levin, L.R. MacDonald, E.J. Hoffman. Investigation of Crystal Geometries for Fiber Coupled Gamma Imaging Intra-operative Probes. This Conference.
- [11] L.R. MacDonald. Beta-Ray Imaging Surgical Scintillation Detector with Visible Light Photon Counter Readout. Ph.D. Thesis, UCLA, 1996.
- [12] RR Raylman, et al. ¹⁸F-Fluorodeoxyglucose-Guided Breast Cancer Surgery with a Positron-Sensitive Probe: Validation in Preclinical Studies. *J. Nuc. Med.* **36**(10) (1995)1869-1874.
- [13] F. Daghighian, J.C. Mazziotta, E.J. Hoffman, et al. Intraoperative Beta Probe: A Device for Detecting Tissue Labeled with Positron or Electron Emitting Isotopes During Surgery. *Med. Phys.* **21**(1) (1994) 153-7.
- [14] See G.F. Knoll. Radiation Detection and Measurement, 2nd Ed., Wiley, NY 1989, p. 326, and references therein.
- [15] M. Bantel, et al. A Two-Dimensional Position Sensitive Phoswich Detector. *Nucl Instr Meth A* **226** (1984) 394-404.